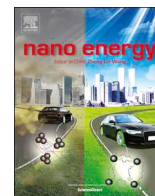




ELSEVIER

Contents lists available at ScienceDirect

Nano Energy

journal homepage: [www.elsevier.com/locate/nanoen](http://www.elsevier.com/locate/nanoen)

Full paper

## Toward a remarkable Li-S battery via 3D printing

Xuejie Gao<sup>a,b,1</sup>, Qian Sun<sup>a,1</sup>, Xiaofei Yang<sup>a</sup>, Jianneng Liang<sup>a</sup>, Alicia Koo<sup>a</sup>, Weihan Li<sup>a,b</sup>, Jianwen Liang<sup>a</sup>, Jiwei Wang<sup>a,b</sup>, Ruying Li<sup>a</sup>, Frederick Benjamin Holness<sup>a</sup>, Aaron David Price<sup>a</sup>, Songlin Yang<sup>c</sup>, Tsun-Kong Sham<sup>b,\*</sup>, Xueliang Sun<sup>a,\*</sup>

<sup>a</sup> Department of Mechanical and Materials Engineering, University of Western Ontario, 1151 Richmond St, London, Ontario N6A 3K7, Canada

<sup>b</sup> Department of Chemistry, University of Western Ontario, London, Ontario N6A 5B7, Canada

<sup>c</sup> Department of Chemical and Biochemical Engineering, University of Western Ontario, 1151 Richmond St, London, Ontario N6A 3K7, Canada



### ARTICLE INFO

#### Keywords:

3D printing  
Self-standing S/BP 2000 cathode  
High sulfur loading  
Li sulfur batteries

### ABSTRACT

We demonstrate the successful application of 3D printing (additive manufacturing) to construct high energy density and power density sulfur/carbon cathodes for Li-S batteries. A self-standing 3D-printed sulfur/carbon cathode with high sulfur loading based on a low-cost commercial carbon black was fabricated via a facile robocasting 3D printing process. The 3D-printed sulfur/carbon cathode shows excellent electrochemical performance in terms of capacity, cycling stability, and rate retention by facilitating Li<sup>+</sup>/e<sup>-</sup> transport at the macro-, micro-, and nano-scale in Li-S batteries. Meanwhile, the areal loading of the sulfur/carbon cathode can be easily controlled by the number of stacking layers during 3D printing process. The Li-S batteries assembled with the 3D-printed sulfur/carbon cathodes with a sulfur-loading of 3 mg cm<sup>-2</sup> deliver a stable capacity of 564 mA h g<sup>-1</sup> within 200 cycles at 3 C. Moreover, cathodes with a sulfur-loading of 5.5 mg cm<sup>-2</sup> show large initial specific discharge capacities of 1009 mA h g<sup>-1</sup> and 912 mA h g<sup>-1</sup>, and high capacity retentions of 87% and 85% after 200 cycles at rates as high as 1 C and 2 C (equaling to high areal current densities of 9.2 mA cm<sup>-2</sup> and 18.4 mA cm<sup>-2</sup>), respectively.

## 1. Introduction

Fabrication of high-performance electrodes plays an important role in improving the electrochemical performance of energy storage devices such as Li-S [1–4], Li-O<sub>2</sub> [5], and Li-ion batteries [6–8], as well as supercapacitors [9–12]. The widely used blade-casting method is restricted to 2D patterned electrodes, thus hindering active material loading and electrochemical performance due to limited ion and electron transport routes [13]. In contrast 3D-printing has recently received increasing attention for its application in the field of battery research for the controlled design of electrodes [14] and electrolytes [15] from the nanoscale to the macroscale. By precisely controlling electrode geometry and structure, 3D printed electrodes can improve ion/electron transport. Moreover, the thickness and active material loading can be easily controlled by adjusting the number of printed electrode layers [16,17]. In other words, 3D-printing is a powerful technique that is capable of fabricating electrodes with high active material loading and improved ion/electron conductivity, and is thereby a promising method to improve the energy and power density of energy storage systems.

3D-printing technology has found wide applications in the fabrication of electrodes for various energy storage systems such as Li-ion batteries (LIBs) [18,19], Zn-O<sub>2</sub> [20], Li-O<sub>2</sub> and Li-S batteries [21,22]. In 2013, a 3D-printed Li-ion battery using Li<sub>4</sub>Ti<sub>5</sub>O<sub>12</sub> (LTO) as the anode and LiFePO<sub>4</sub> (LFP) as the cathode was fabricated by Dillon's and Lewis's groups. Due to its high active material loading and excellent capacity output, the micro-battery delivered high areal capacities of 4.45 mA h cm<sup>-2</sup> at 0.14 mA cm<sup>-2</sup> (equaling to a volumetric capacity of 17.3 Ah L<sup>-1</sup>), while corresponding full cells delivered 14.5 mA h cm<sup>-2</sup> at 0.2 mA cm<sup>-2</sup> (corresponding to an energy density of 20 mW h cm<sup>-2</sup> at a power density of 1 mW cm<sup>-2</sup>). More recently, a 3D printed sulfur copolymer-graphene electrode has been fabricated based on an ink composed of sulfur particles, 1, 3-diisopropenylbenzene (DIB), and condensed graphene oxide [22]. The 3D printing process was carried out through an extrusion-based 3D printing approach and was successfully implemented as a free-standing cathode for Li-S batteries with a grid structure. This previous study demonstrated the benefit of the application of 3D printing in the fabrication of thick sulfur cathodes, where a thickness of 600 μm was easily realized by stacking 6 printed

\* Corresponding authors.

E-mail addresses: [tsham@uwo.ca](mailto:tsham@uwo.ca) (T.-K. Sham), [xsun9@uwo.ca](mailto:xsun9@uwo.ca) (X. Sun).

<sup>1</sup> Xuejie Gao and Qian Sun contributed equally to this work.

<https://doi.org/10.1016/j.nanoen.2018.12.001>

Received 12 August 2018; Received in revised form 19 October 2018; Accepted 2 December 2018

Available online 03 December 2018

2211-2855/ © 2018 Published by Elsevier Ltd.

layers. However, limited by the low electronic conductivity of the sulfur copolymer, this reported Li-S battery based on the 3D printed sulfur-polymer cathode delivered a relatively low initial capacity of  $812.8 \text{ mA h g}^{-1}$  and exhibited a low capacity retention of 43.4% within 50 cycles at  $50 \text{ mA g}^{-1}$ . In addition, the rate performance was also insufficient, exhibiting a capacity of  $186 \text{ mA h g}^{-1}$  at  $800 \text{ mA g}^{-1}$  (0.5 C). Accordingly, both the cycling stability and C-rate performance are not yet competitive compared to the recently reported high sulfur loading Li-S batteries using traditional fabrication methods [23–27]. Therefore, further optimization of the 3D printing process is still in necessary to improve electrode architecture to ensure high electronic and ionic conductivity, while preferably using low cost and scalable materials. These properties will be imperative in the development of 3D-printed Li-S batteries with superior electrochemical performance (e.g. sulfur utilization, C-rate performance and cycling stability).

Herein, we demonstrate the use of 3D printing (additive manufacturing) to construct a self-standing high areal energy density cathode for Li-S battery based on a sulfur/carbon composite, which demonstrates superior electrochemical performance. A low-cost commercial carbon black (BP-2000) containing abundant micro-pores is chosen as the host material for sulfur to fabricate the sulfur/carbon (S/C) cathode. The ink for 3D printing is composed of the S/C active material, acetylene black (AB) and commercial carbon nanotubes (CNTs) as the conductive additives, and polyvinylidene fluoride-hexafluoro propylene (PVDF-HFP) as the binder dissolved in 1-methyl-2-pyrrolidinone (NMP). The porosity and conductivity of the electrode structure is further optimized from the macroscale to the nanoscale by (1) 3D-printing a porous structure with macro-sized pores (several hundred micrometers), (2) phase inversion of the polymeric binder to produce pores between several micrometers to nanometers in size, and (3) selecting materials with a microporous structure (less than 2 nm). Moreover, two critical post-treatment steps after 3D printing involve phase inversion and freeze drying to significantly elevate the electrochemical performance of the final 3D printed S/C electrode with hierarchical porous structure enabling facile electronic and ionic transportation. As a result, a superior Li-S battery containing high sulfur loading S/C cathodes with excellent C-rate performance and cycling stability are realized via 3D printing. The Li-S batteries assembled with approximately  $3 \text{ mg cm}^{-2}$  sulfur-loaded 3D printed-freeze dried electrode (referred to as 3DP-FDE) delivers a stable capacity of  $564 \text{ mA h g}^{-1}$  within 200 cycles at 3 C. The  $5.5 \text{ mg cm}^{-2}$  sulfur-loaded 3DP-FDE, shows high initial discharge specific capacities of  $1009 \text{ mA h g}^{-1}$  and  $912 \text{ mA h g}^{-1}$ , and capacity retentions of 87% and 85% within 200 cycles at high C-rates of 1 C and 2 C, respectively.

## 2. Experimental section

### 2.1. Synthesis of S/BP-2000 composite

1200 mg of sulfur powder (99.5%, Sigma-Aldrich) was mixed with conductive carbon (Cabot BP-2000) with a weight ratio of 6:4, then ground with mortar and pestle for 0.5 h. The mixture was then transferred to a sealed steel reactor and was heated at  $155 \text{ }^\circ\text{C}$  for 8 h followed by  $300 \text{ }^\circ\text{C}$  for 4 h. After cooling to room temperature, the final S/BP-2000 composite with a sulfur content of 60 wt% was obtained.

### 2.2. Preparation of 3DP-FED and 3DP-ODE

3D-printed S/BP-2000 cathode was fabricated using a custom-made 3D printer equipped with a 3-axis micropositioning stage (FFF Delta 3D printer) motorized by stepper motors (CNC4PC, CS4EA4-1Rev1). The printing process is as follows: S/BP-2000 composite, PVDF-HFP, carbon nanotubes (CNTs, diameter of 40–60 nm, length of 2  $\mu\text{m}$ ), and acetylene black with a weight ratio of 7:2:0.5:0.5 were first mixed with 1-methyl-2-pyrrolidinone (NMP) to form an ink. The as-prepared ink was then

loaded into a 3 mL syringe and extruded through a 150  $\mu\text{m}$  diameter nozzle. The 3D-printed S/BP-2000 cathodes were printed with a diameter of 10 mm at a print motion speed of  $6 \text{ mm s}^{-1}$ . The printed electrode use two different treatments for comparison: 1) Firstly, printed electrodes were immediately immersed in a water (100 mL) coagulation bath for 5 min. It is noted that it performed phase inversion during this process. The binder network, electron paths and ion channels formed during phase inversion can significantly improve adhesive strength, facilitate electron/ion transport [13,28]. After that, freeze-dried at  $-50 \text{ }^\circ\text{C}$  was applied to maintain the structure formed during 3D printing and phase inversion. The obtained electrode named as 3DP-FDE. 2) For comparison, the printed electrode directly dried in a  $60 \text{ }^\circ\text{C}$  oven for 18 h, labelled as 3DE-ODE.

### 2.3. Synthesis of CP@NCNT

N-doped carbon nanotubes were synthesized by a spray pyrolysis chemical vapor deposition (SPCVD) method based on previous reports [29]. ALD coatings were conducted on carbon paper (CP) in a Gemstar-8 ALD system (Arradance, USA).  $\text{Al}_2\text{O}_3$  was deposited on the CP at  $120 \text{ }^\circ\text{C}$  by using trimethylaluminium (TMA) and water ( $\text{H}_2\text{O}$ ) as precursors for 200 cycles. Then, the  $\text{Al}_2\text{O}_3$  coated CP ( $2 \times 8 \text{ cm}^{-2}$ ) was loaded into a vertical tube furnace that was ramped from room temperature to  $856 \text{ }^\circ\text{C}$  under  $200 \text{ mL min}^{-1}$  Ar flow. A catalytic ferrocene solution (solvent: acetonitrile, concentration:  $0.02 \text{ g mL}^{-1}$ ) was subsequently introduced into the quartz tube at a flow rate of  $0.1 \text{ mL min}^{-1}$  for 5 min under Ar atmosphere. Following this, imidazole solution was injected into the quartz tube (solvent: acetonitrile, concentration:  $0.2 \text{ g mL}^{-1}$ , flow rate:  $0.1 \text{ mL min}^{-1}$ ) to grow NCNT bundles for 30 min followed by cooling to room temperature. Typically, 30 min of growth yielded NCNT bundles with a length of approximately 20–40  $\mu\text{m}$ .

### 2.4. Characterization

The morphologies of the samples were characterized by a Hitachi S-4800 field emission scanning electron microscope (FE-SEM). The sulfur content in the S/BP 2000 composite was determined by a SDT Q600 thermogravimetric analyzer (TGA) under a nitrogen atmosphere from room temperature to  $600 \text{ }^\circ\text{C}$  with a heating rate of  $10 \text{ }^\circ\text{C min}^{-1}$ . Raman (HORIBA Scientific LabRAM) spectra were recorded to evaluate the graphitic degree of carbon materials.

### 2.5. Electrochemical measurements

The electrochemical performance of the 3D-printed S/BP 2000 cathodes were tested with CR2032 coin cells, constructed in an Ar-filled glovebox. The cathode and Li anode were separated by a polypropylene membrane (Celgard 2400). A CP@NCNT interlayer was used between the separator and the cathode to improve the active material utilization capacity retention as well. The interlayer is beneficial for providing fine contact with the cathode surface, offering electron pathways through the insulating S/Li<sub>2</sub>S and accommodating the migrating polysulfide intermediates [25,30,31]. The electrolyte used in this study was 1 M bis(trifluoromethylsulfonyl) imide (LiTFSI) in 1,2-dimethoxyethane (DME) /1, 3-dioxolane (DOL) (1:1 v/v) with 1 wt%  $\text{LiNO}_3$  additive, and the electrolyte/sulfur (E/S) ratio is controlled as around  $22 \mu\text{L mg}^{-1}$  for both 3DP-FDE and 3DP-ODE electrodes.

Electrochemical impedance spectroscopy (EIS) was tested at open-circuit with a frequency range of  $5.0 \times 10^5 \text{ Hz}$  to  $1.0 \times 10^{-2} \text{ Hz}$  on a versatile multichannel potentiostation 3/Z (VMP3). Cyclic voltammetry (CV) was performed on the same instrument and the data was collected under a scanning rate of  $0.1 \text{ mV s}^{-1}$  between 1.8 V and 2.8 V. The charge-discharge tests were carried out using a LAND CT-2001A system with voltages between 1.8 V and 2.8 V at room temperature. Unless otherwise specified, the specific capacities reported in this work were

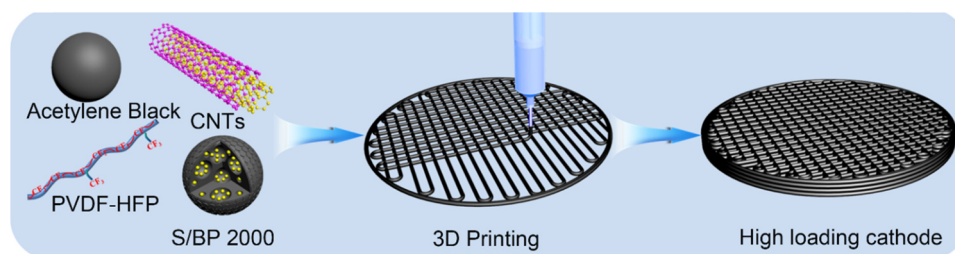


Fig. 1. Schematic illustration of the 3D-printing process for S/BP 2000 thick cathodes (the diameter of printed grid electrode is 10 mm).

calculated based on sulfur and the voltages vs.  $\text{Li}^+/\text{Li}$ .

### 3. Results and discussion

The 3D printing fabrication of the S/BP-2000 electrode is summarized in Fig. 1; it involves three main stages: (1) ink preparation, (2) 3D printing, and (3) post treatment (phase inversion and freeze drying). The cathode ink is first prepared by dispersing the S/BP 2000 composite with carbon nanotubes (CNTs) and acetylene black as conductive additives in a PVDF-HFP solution with NMP as solvent. The ink is then transferred into a syringe and printed in various patterns by a 3D printer. The as-printed electrode is finally treated by phase inversion in  $\text{H}_2\text{O}$  followed by further removal of the solvent in the ink via a freeze-drying method to obtain a freestanding and flexible sulfur cathode.

The 3D printed structure of the cathode is designed to improve  $\text{Li}^+/\text{e}^-$  transport and active material loading. The as-prepared 3D printed freeze-dried electrode is fabricated by extrusion into a well-controlled grid pattern at the macroscale, as shown in Fig. 1. Electrons can be transported along the extruded filament, which shortens the transport distance and improves electronic conductivity, while the pores among the fibers are beneficial for electrolyte accommodation and  $\text{Li}^+$  transport at the macroscale. The  $\text{Li}^+/\text{e}^-$  transport at the nanoscale is further improved by the continuous  $\text{Li}^+$  transport channels and  $\text{e}^-$  paths formed via phase inversion according to previous reports [13]. It is important to note that high sulfur loading cathodes are easily fabricated by increasing the number of printed electrode layers, allowing for applications in high-energy-density Li-S batteries. Moreover, 3D-printing has also proved to be an efficient strategy to control the geometric and architectural structure to meet the demand of different flexible devices [17,32]. As shown in Fig. S1, different shapes, fill patterns, and even individual fibers can be successfully printed.

To highlight the advantages of 3D-printing for the fabrication of high sulfur loading cathodes, the widely used blade-casting method was chosen for comparison. As shown in Fig. 2a, the blade-casting slurry was uniformly coated on the surface of an Al foil. Unfortunately, the high areal sulfur loading electrode cracked after drying in a vacuum oven at  $60^\circ\text{C}$  and delaminated from the current collector, thus damaging the electron transport network and limiting the active material loading (Fig. 2d and g). In contrast, the 3D-printed S/C electrode shows a clear grid structure before drying, which is coated on a glass substrate (Fig. 2b-c). The structure of the printed electrodes is well maintained after both oven drying at  $60^\circ\text{C}$  (referred to as 3DP-ODE) and freeze-drying (referred to as 3DP-FDE), shown in Fig. 2e-f, revealing the merits of 3D-printing for the preparation of high sulfur loading cathodes. It is noteworthy that the 3DP-ODE shrunk when dried in a vacuum oven, mainly resulting from surface tension, which is detrimental to electrolyte accommodation and  $\text{Li}^+/\text{e}^-$  transport. Freeze-drying is known to be an efficient strategy to avoid the shrinking caused by surface tension by utilizing low temperature and high vacuum conditions [33,34]. As shown in Fig. 2i, the 3DP-FDE shows no obvious shrinkage during the freeze-drying process and the grid structure is well maintained. This is beneficial for accommodating the electrolyte, improving the mechanical strength and flexibility (Fig. 2i), and likely facilitating the  $\text{Li}^+/\text{e}^-$

transport from the macroscale to the nanoscale.

The appearance and morphology of the 3DP-FDE is shown in Fig. 3. The 3DP-FDE is fabricated with a grid structure with a diameter of  $150\ \mu\text{m}$  composed of interwoven fibers that can facilitate electron transport, shown in Fig. 3a-b. It can also be observed that the distance between two adjacent fibers is  $150\ \mu\text{m}$ , which results in uniformly distributed square pores. Those pores can serve as  $\text{Li}^+$  transport channels as well as provide enough space for electrolyte accommodation at the macroscale. From the cross-sectional view, as shown in Fig. 3c, the thickness of a single printed layer of 3DP-FDE is  $150\ \mu\text{m}$ , corresponding to a sulfur loading of  $1.3\text{--}1.5\ \text{mg cm}^{-2}$ . When increased to four printed layers, a 3DP-FDE with a thickness of  $600\ \mu\text{m}$  and sulfur loading of  $5.5\ \text{mg cm}^{-2}$  is obtained, shown in Fig. 3d. These results demonstrate the precision of a layer-by-layer manufacturing process and indicate that a S/C electrode with a high sulfur loading of around  $5.5\ \text{mg cm}^{-2}$  can be realized by 3D printing technology to meet the demand of high energy density Li-S batteries.

The micro and nanopores form part of a homogenous “tri-continuous” phase structure containing the polymeric binder and the S/C composite, shown in Fig. 3e-f. According to previous reports [13], this “tri-continuous” phase behaves as a continuous binder network with conductive electron paths and interconnected ion channels, which is beneficial for increasing adhesive strength and facilitating electron/ion transport at the nanoscale. On the contrary, as shown in Fig. S2, due to electrode shrinkage caused by surface tension, there are no obvious pores at the nanoscale exhibited in 3DP-ODE, which is detrimental to electrolyte accommodation and  $\text{Li}^+$  transport. In this consideration, the 3DP-FDE shows excellent  $\text{Li}^+/\text{e}^-$  transport capability from the macroscale to the nanoscale, which is beneficial to improve the C-rate performance of high sulfur loading cathodes, enabling high energy density Li-S batteries with high power density. Additionally, the micro-pores in BP-2000, nanoscale pores throughout the S/BP-2000 composite formed during phase inversion, and macroscale pores fabricated by 3D-printing can anchor the well-located polysulfides in the cathode, thus relieving the shuttling effect and improving the cycling stability [23,35]. The homogeneity of the electrode is further confirmed by EDX and elemental mapping images, indicating that S, C, O and F are uniformly distributed inside the 3DP-FDE (Fig. 3g-i). Thermogravimetric analysis (TGA) reveals that the sulfur content in S/BP 2000 composite is 60 wt% as shown in Fig. S3. Furthermore, Raman analysis was carried out to investigate the carbon structure of 3DP-FDE (Fig. S4). The Raman spectrum presents two characteristic peaks located at approximately  $1336.56\ \text{cm}^{-1}$  and  $1579.65\ \text{cm}^{-1}$ , which is related to the D and G bands of carbon, respectively. The D-band represents  $\text{sp}^3$  C-C bonds (defect) and the G-band planar  $\text{sp}^2$  C-C bonds [36,37].

The cyclic voltammograms (CV) of 3DP-FDE and 3DP-ODE electrodes with sulfur loadings of approximately  $3\ \text{mg cm}^{-2}$  are obtained at a scan rate of  $0.1\ \text{mV s}^{-1}$  between 1.8 V and 2.8 V. As shown in Fig. S5a, Li-S CV profiles of typical oxidation and reduction peaks are presented in the selected voltage window. For the 3DP-FDE electrode, the first reduction peak at 2.34 V is mainly attributed to the reduction of  $\text{S}_8$  to long-chain lithium polysulfides ( $\text{Li}_2\text{S}_x$ ,  $x \geq 4$ ). The second reduction peak at 2.00 V is caused by the further reduction of long-chain lithium

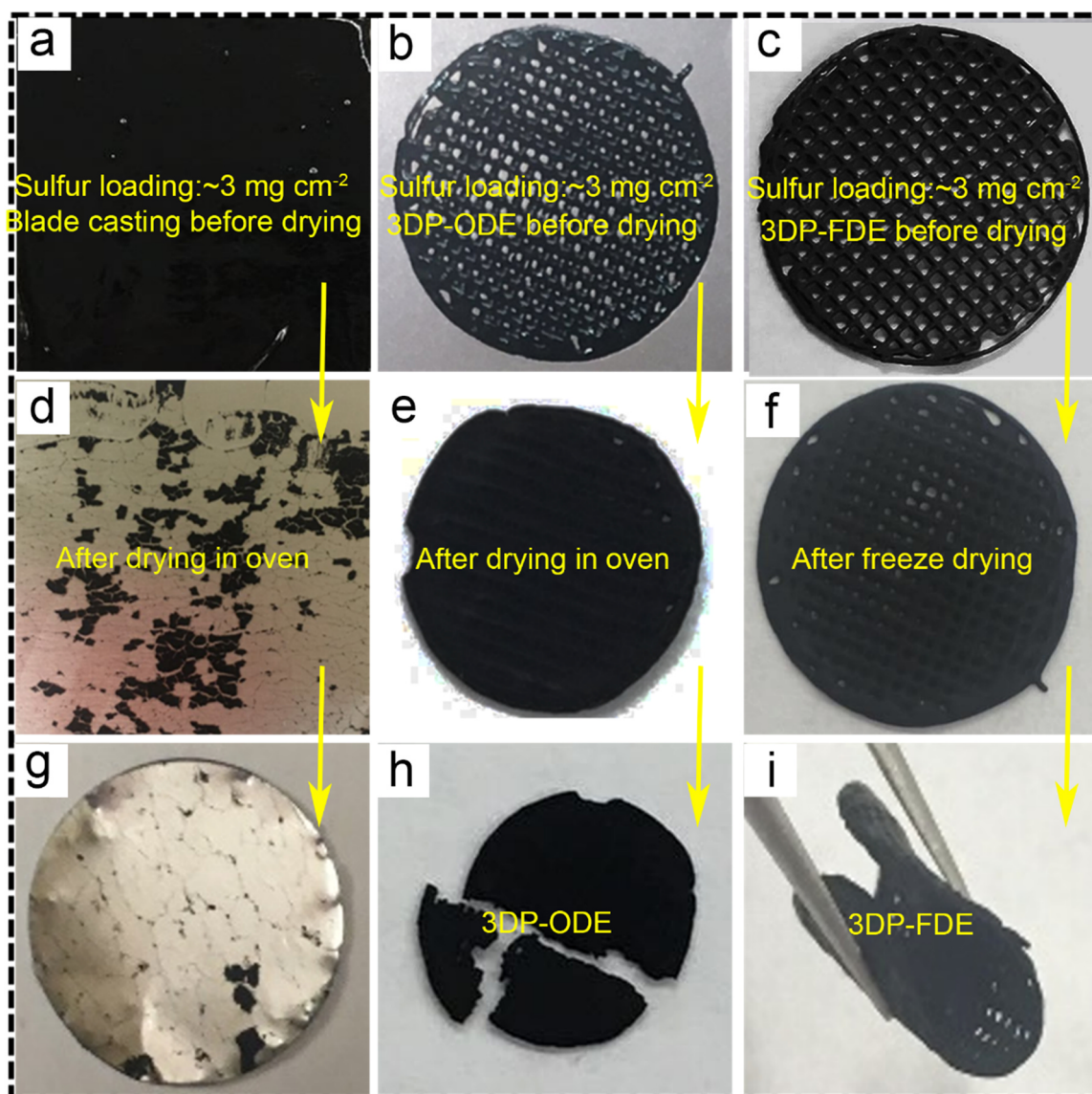


Fig. 2. Optical images S/BP 2000 cathodes before and after drying with different methods.

polysulfides to shorter polysulfides ( $\text{Li}_2\text{S}_x$ ,  $1 < x < 4$ ) and  $\text{Li}_2\text{S}$  [38,39]. In addition, there are two oxidation peaks located at 2.34 V and 2.43 V, corresponding to the two-step oxidation of lithium sulfide ( $\text{Li}_2\text{S}$ ) to sulfur [40]. However, for the 3DP-ODE, the oxidation peaks shift to higher voltages (2.36 V and 2.47 V) and reduction peaks shift to lower voltages (2.28 V and 1.96 V), as well as the area of this curve is smaller than that of 3DP-FDE, demonstrating increased polarization. After the first cycle, as shown in Fig. S5b, all CV curves overlap with each other, suggesting suppressed polysulfide shuttling and excellent cycling performance. Such large differences in the electrochemical reaction kinetics can be attributed to the difference in  $\text{Li}^+/\text{e}^-$  conductivity between the two drying methods, which is further verified by EIS measurements as shown in Fig. S5c and Fig. S5d. These results suggest higher electrochemical activity and faster  $\text{Li}^+$  diffusion [41] and further highlights the increased active sites and improved  $\text{Li}^+$  transport channels at both the micro and nanoscale in the 3DP-FDE as a result of coupling 3D-printing and freeze drying techniques during electrode fabrication.

The electrochemical performance of 3DP-FDE with high sulfur loadings of  $3 \text{ mg cm}^{-2}$  and  $5.5 \text{ mg cm}^{-2}$  are studied. The C-rate

performance of the cells assembled with  $3 \text{ mg cm}^{-2}$  sulfur loaded 3DP-FDE at various C-rate from 0.2 C to 3 C is shown in Fig. 4a. After the irreversible capacity decay in the first few cycles at 0.2 C, a stable state is reached and reversible average discharge specific capacities of  $1172 \text{ mA h g}^{-1}$ ,  $838 \text{ mA h g}^{-1}$ ,  $792 \text{ mA h g}^{-1}$ ,  $667 \text{ mA h g}^{-1}$ ,  $534 \text{ mA h g}^{-1}$  are delivered at 0.2 C, 0.5 C, 1 C, 2 C and 3 C, respectively. When the C-rate is returned to 0.2 C, a specific discharge capacity of  $917 \text{ mA h g}^{-1}$  is recovered, suggesting good reversibility of the 3DP-FDE. Fig. 4b shows the charge/discharge profiles between 1.8 V and 2.8 V where two stable plateaus can be observed at all C-rates, suggesting a kinetically efficient process [35]. The excellent C-rate performance for such high sulfur loading cathodes is mainly attributed to the fast electron transport network (shortened electron transport distance along printed fibers and excellent electron conductive network throughout the continuous S/C phase) and excellent electron conductive network (the interconnected  $\text{Li}^+$  transport channels supplied by the 3D printed square pores and continuous pore structures formed during phase inversion), which is meaningful to pave the way for high-energy-density and high-power density Li-S batteries.

The long-term cycling stability of the cells assembled with 3 mg

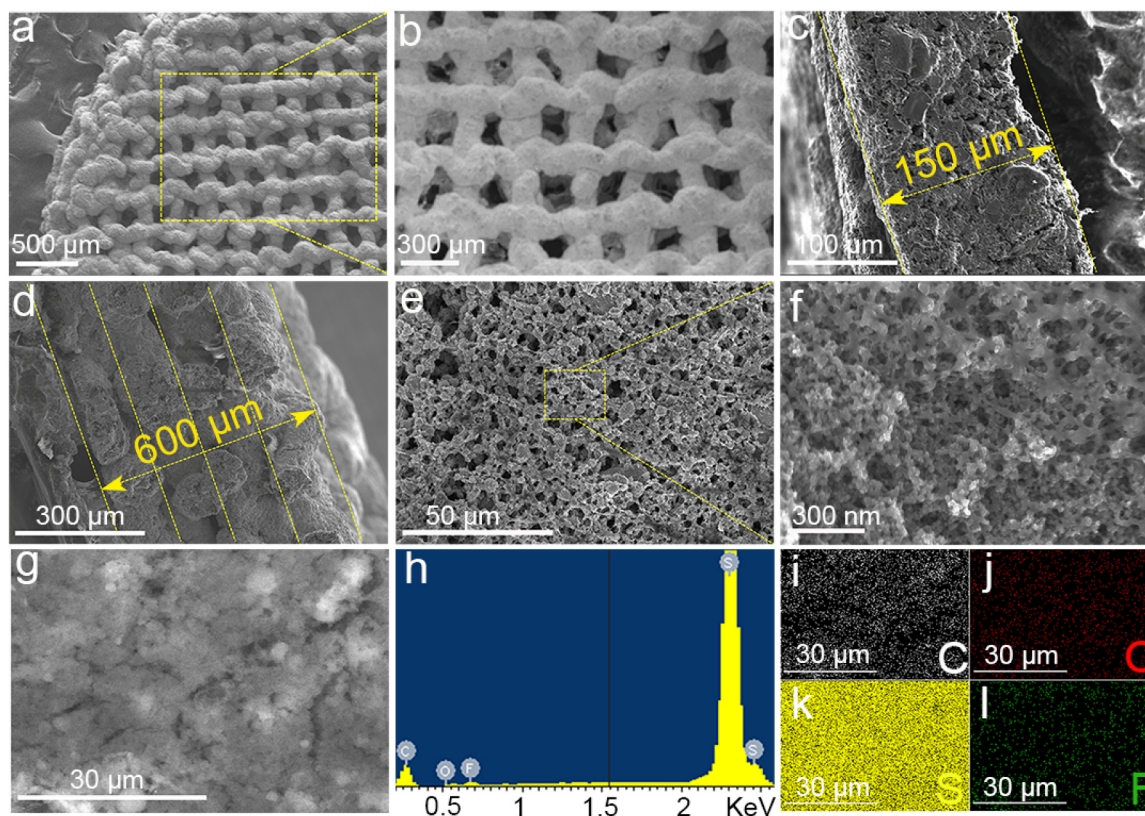


**Fig. 3.** SEM images of 3DP-FDE. a-b) Top view of the electrode at different magnifications. c-d) Cross-sectional view of one layer and four layer thick 3D printed cathodes, respectively. e-f) Continuous micro  $\text{Li}^+/\text{e}^-$  and nanopores of the 3DP-FDE. g-i) Elemental mapping and EDX images of the 3DP-FDE.

$\text{cm}^{-2}$  3DP-FDE at 0.2 C and 3 C is investigated. As shown in Fig. 4c, the cells deliver high initial discharge capacities of  $1184 \text{ mA h g}^{-1}$  and  $940 \text{ mA h g}^{-1}$ , corresponding to high sulfur utilizations of 71% and 56%, respectively. After serious attenuation in the first few cycles, the cells maintain reversible discharge specific capacities of  $856 \text{ mA h g}^{-1}$  and  $812 \text{ mA h g}^{-1}$  at the 10th cycle. Even after 200 cycles, capacities of  $752 \text{ mA h g}^{-1}$  and  $564 \text{ mA h g}^{-1}$  remain, corresponding to 87.9% and 69.4% capacity retention (calculated based on the 10th cycle), respectively. On the contrary, the 3DP-ODE delivers an initial discharge specific capacity of  $1093 \text{ mA h g}^{-1}$  and rapidly decays to  $106 \text{ mA h g}^{-1}$  after 100 cycles at 0.2 C (Fig. S6).

Additionally, the cycling performance of 3DP-FDE with a sulfur loading of  $5.5 \text{ mg cm}^{-2}$  at various C-rates of 0.1 C, 0.5 C, 1 C and 2 C are studied. As shown in Fig. 4d, the cell delivers a high initial capacity of  $1188 \text{ mA h g}^{-1}$  at 0.1 C and a reversible capacity of  $926 \text{ mA h g}^{-1}$  is achieved at the 7th cycle after fast capacity decay in the first few cycles. Even after 100 cycles, still a high capacity of  $802.4 \text{ mA h g}^{-1}$  is maintained, corresponding to a low capacity attenuation rate of 0.14% per cycle (calculated based on the 7th cycle), demonstrating the excellent cycling stability [42,43]. What's more, the cells assembled with the  $5.5 \text{ mg cm}^{-2}$  3DP-FDE operated at higher C-rates of 0.5 C, 1 C, 2 C, equaling to high areal current densities of  $4.6 \text{ mA cm}^{-2}$ ,  $9.2 \text{ mA cm}^{-2}$  and  $18.4 \text{ mA cm}^{-2}$ , still deliver high initial specific capacities of  $1044 \text{ mA h g}^{-1}$ ,  $1009 \text{ mA h g}^{-1}$  and  $912 \text{ mA h g}^{-1}$ , respectively. After serious irreversible capacity decay in the first 10 cycles, stable capacities of  $765 \text{ mA h g}^{-1}$ ,  $748 \text{ mA h g}^{-1}$  and  $722 \text{ mA h g}^{-1}$  are retained. After 200 cycles, the specific capacities are  $626 \text{ mA h g}^{-1}$ ,  $606 \text{ mA h g}^{-1}$  and  $563 \text{ mA h g}^{-1}$ , equaling to capacity retentions of 82%, 81% and 78%, demonstrating excellent cycling stability of the 3DP-FDE with high sulfur loading. The Ragone plot shows that 3DP-FDE compare favorably to values previously reported for other 3D printing electrode,

including those based lithium ion batteries (Fig. S7) [18,44–46]. Our 3DP-FDE delivers an impressive areal capacity that exceeds the reported values of several other 3D printing lithium ion batteries.

The excellent cycling stability of the 3DP-FDE with high sulfur loading can be attributed to the optimized ionic and electronic conductivity of the cathode material, as the unique advantage of the application of 3D printing fabrication technology, as summarized in Fig. 5. The printed cathode shows an ideal macro-scale grid structure for  $\text{Li}^+/\text{e}^-$  transport with increased surface area, facilitating the electrochemical reactions between the surface of the cathode and electrolyte, which results in high sulfur utilization and high discharge capacity output. In addition, the macropores of the grid structure, micropores in BP-2000, and nanopores formed during phase inversion of the binder can anchor the well-located polysulfides in the cathode, thus relieving the shuttling effect and improving the cycling stability. These presented results are expected to open a new area for designing Li-S batteries with high energy and power density based on 3D printing technology, and may shed light on the research and development of other energy storage devices including Li-ion and Li- $\text{O}_2$  batteries.

#### 4. Conclusion

In summary, we developed a 3D-printed freeze-dried S/C composite electrode (3DP-FDE) via a facile layer-by-layer manufacturing process based on low-cost commercial BP-2000 carbon material for high-energy-density and high-power-density Li-S batteries. The 3DP-FDE is fabricated with well-controlled extruded fibers. The electrons can be transported along the fibers, which shortens electron transport distance, while the microscale pores among the fibers is beneficial for electrolyte accommodation and  $\text{Li}^+$  transport in microscale. The electrode structure is further optimized with phase inversion, where the transport of

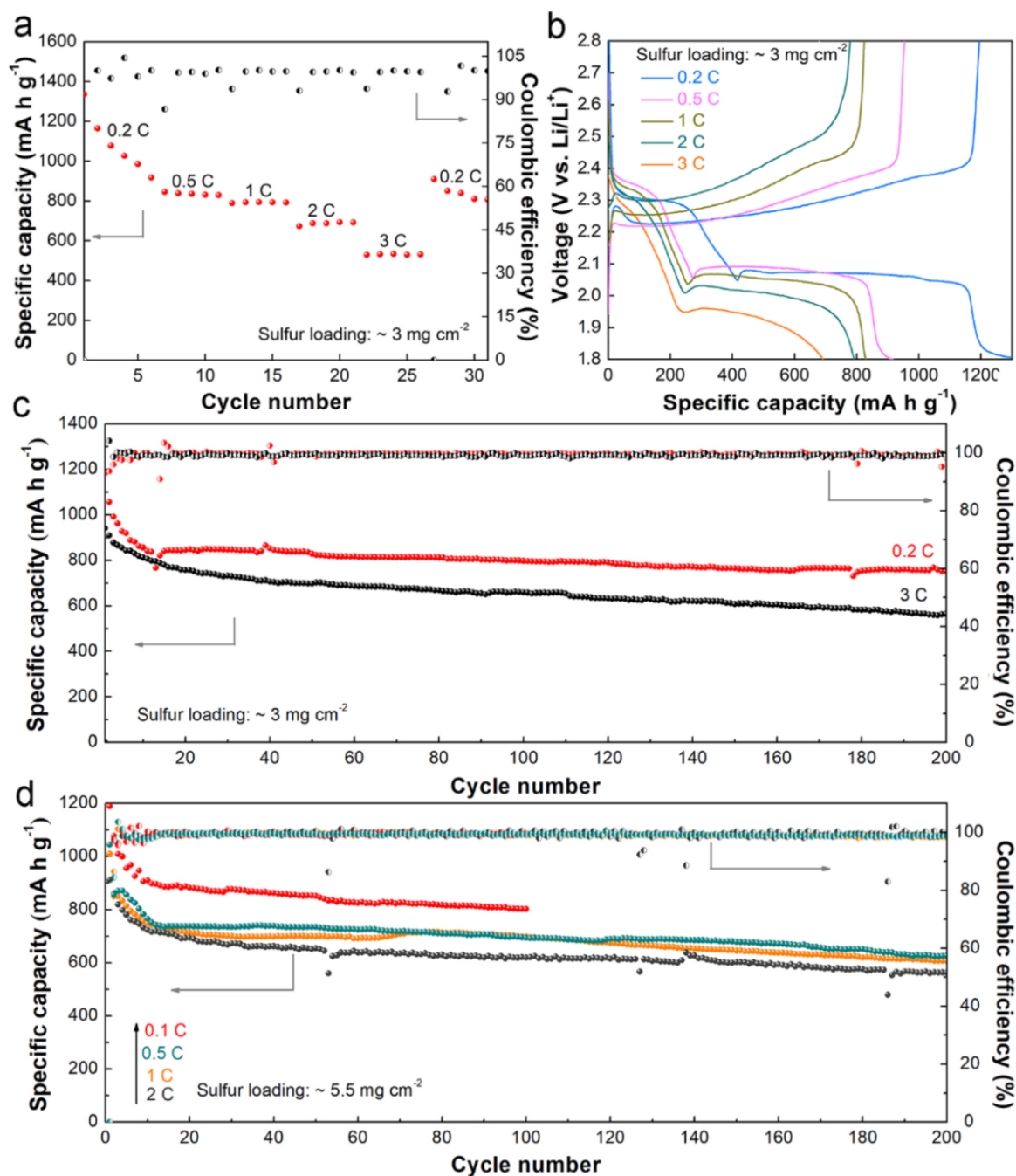


**Fig. 4.** Cycling performance of Li-S cell assembled with 3DP-FDE. a) C-rate performance of Li-S cells assembled with a sulfur loading of  $3 \text{ mg cm}^{-2}$  at various C-rate between 0.2 and 3 C and b) charge/discharge profiles. c) Cycling performance of Li-S cells assembled with 3DP-FDE with a sulfur loading of  $3 \text{ mg cm}^{-2}$  at 0.2 C and 3 C. d) Cycling performance of Li-S cells assembled with 3DP-FDE with a sulfur loading of  $5.5 \text{ mg cm}^{-2}$  at 0.1 C, 0.5 C, 1 C and 2 C.

Li<sup>+</sup>/e<sup>-</sup> at the nanoscale is further improved by the formation of a continuous porous structure and interconnected S/BP 2000 composite phase. What's more, the micropores in BP 2000, nanoscale pores among S/BP 2000 composite formed during phase inversion process, and microscale pores fabricated by 3D printing can anchor the well-located polysulfides in the cathode, thus relieving the shuttling effect. By addressing Li<sup>+</sup>/e<sup>-</sup> transport and suppressing polysulfide shuttling, excellent C-rate performance and cycling stability of high sulfur loaded 3DP-FDE are exhibited. The Li-S batteries assembled with  $3 \text{ mg cm}^{-2}$  sulfur-loaded 3DP-FDE deliver a high capacity of  $534 \text{ mA h g}^{-1}$  at 3 C and high stable and reversible discharge specific capacities of

$752 \text{ mA h g}^{-1}$  and  $564 \text{ mA h g}^{-1}$  are retained after 200 cycles at C-rates of 0.2 C and 3 C. For the  $5.5 \text{ mg cm}^{-2}$  sulfur-loaded 3DP-FDE, they show high initial discharge specific capacities of  $1009 \text{ mA h g}^{-1}$  and  $912 \text{ mA h g}^{-1}$ , and capacity retentions of 87% and 85% within 200 cycles at high C-rates of 1 C and 2 C (equaling to high areal current densities of  $9.2 \text{ mA cm}^{-2}$  and  $18.4 \text{ mA cm}^{-2}$ ), respectively. Overall, this work offers a new strategy to fabricate high sulfur loading cathodes and improve the electrochemical performance including cycling stability and rate performance for advanced Li-S batteries, which could pave the way for the practical application of high-energy-density and high-power-density Li-S batteries.

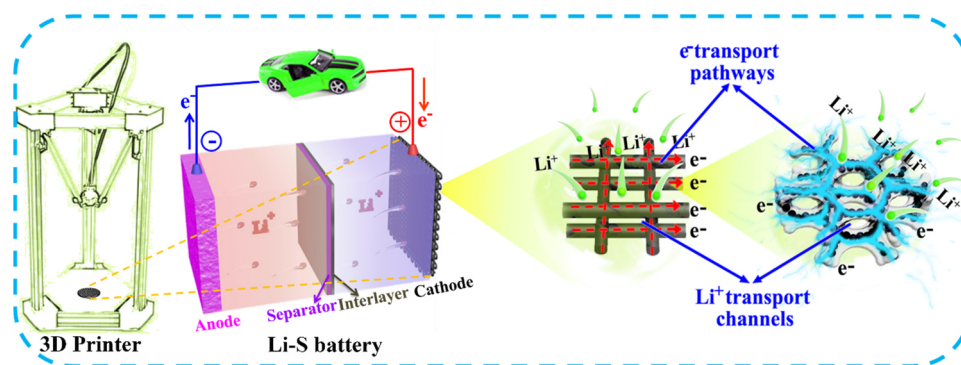


Fig. 5. Schematic illustration of 3DP-FDE applied in Li-S batteries with excellent  $\text{Li}^+$ / $\text{e}^-$  transport in both micro- and nano-scale.

## Acknowledgements

This research was supported by the Natural Science and Engineering Research Council of Canada (NSERC), the Canada Research Chair Program (CRC), the Canada Foundation for Innovation (CFI), and the University of Western Ontario (UWO). Xuejie Gao is supported by the China Scholarship Council.

## Supporting information

Supporting information is available from the Wiley Online Library or from the author.

## Author contribution

X. G. and Q. S. contributed equally to this work. X. S. and T.-K. S. directed the project. X. G., Q. S. and X. Y. conceived the idea and designed the experiments of this work. X. G. did all experiment of this work. J. L. did the SEM characterization. A. K. edited the language. W. L. did the SEM mapping. J. L. provided the Raman test. J. W. helped some 3D printing test. R. L. assisted with purchasing chemicals. The 3D printer was cooperated by A. D. P. group (Including the student F. B. H.) and X. S. group. S. Y. helped freeze drying. X. G. wrote the original manuscript. All authors discussed the results and reviewed this manuscript.

## Declaration of interests

The authors declare no competing interests.

## Appendix A. Supporting information

Supplementary data associated with this article can be found in the online version at [doi:10.1016/j.nanoen.2018.12.001](https://doi.org/10.1016/j.nanoen.2018.12.001).

## References

- X. Ji, K.T. Lee, L.F. Nazar, *Nat. Mater.* 8 (2009) 500–506.
- X. Yang, N. Yan, W. Zhou, H. Zhang, X. Li, H. Zhang, *J. Mater. Chem. A* 3 (2015) 15314–15323.
- X. Yang, X. Li, K. Adair, H. Zhang, X. Sun, *Electrochem. Energy Rev.* 1 (2018) 239–293.
- X. Yang, Y. Yu, X. Lin, J. Liang, K. Adair, Y. Zhao, C. Wang, X. Li, Q. Sun, H. Zhang, X. Li, R. Li, H. Zhang, X. Sun, *J. Mater. Chem. A* 6 (2018) 22958–22965, <https://doi.org/10.1039/C8TA08188C>.
- P.G. Bruce, S.A. Freunberger, L.J. Hardwick, J.M. Tarascon, *Nat. Mater.* 11 (2012) 19–29.
- X. Gao, J. Wang, D. Zhang, K. Adair, K. Feng, N. Sun, H. Zheng, H. Shao, J. Zhong, Y. Ma, X. Sun, X. Sun, *J. Mater. Chem. A* 5 (2017) 25625–25631.
- X. Gao, J. Wang, D. Zhang, K. Nie, Y. Ma, J. Zhong, X. Sun, *J. Mater. Chem. A* 5 (2017) 5007–5012.
- Y. Wang, C. Chen, H. Xie, T. Gao, Y. Yao, G. Pastel, X. Han, Y. Li, J. Zhao, K. Fu, L. Hu, *Adv. Funct. Mater.* 27 (2017) 1703140.
- B. Li, F. Dai, Q. Xiao, L. Yang, J. Shen, C. Zhang, M. Cai, *Adv. Energy Mater.* 9 (2016) 102–106.
- H. Wang, Z. Xu, Z. Li, K. Cui, J. Ding, A. Kohandehghan, X. Tan, B. Zahiri, B.C. Olsen, C.M. Holt, D. Mitlin, *Nano Lett.* 14 (2014) 1987–1994.
- R. Yi, S. Chen, J. Song, M.L. Gordin, A. Manivannan, D. Wang, *Adv. Funct. Mater.* 24 (2014) 7433–7439.
- K.H. Choi, J. Yoo, C.K. Lee, S.-Y. Lee, *Energy Environ. Sci.* 9 (2016) 2812–2821.
- X. Yang, Y. Chen, M. Wang, H. Zhang, X. Li, H. Zhang, *Adv. Funct. Mater.* 26 (2016) 8427–8434.
- H. Lin, W. Weng, J. Ren, L. Qiu, Z. Zhang, P. Chen, X. Chen, J. Deng, Y. Wang, H. Peng, *Adv. Mater.* 26 (2014) 1217–1222.
- A.J. Blake, R.R. Kohlmeier, J.O. Hardin, E.A. Carmona, B. Maruyama, J.D. Berrigan, H. Huang, M.F. Durstock, *Adv. Energy Mater.* 7 (2017) 1602920.
- C. Zhu, T. Liu, F. Qian, W. Chen, S. Chandrasekaran, B. Yao, Y. Song, E.B. Duoss, J.D. Kuntz, C.M. Spadaccini, M.A. Worsley, Y. Li, *Nano Today* 15 (2017) 107–120.
- F. Zhang, M. Wei, V.V. Viswanathan, B. Swart, Y. Shao, G. Wu, C. Zhou, *Nano Energy* 40 (2017) 418–431.
- T.S. Wei, B.Y. Ahn, J. Grotto, J.A. Lewis, *Adv. Mater.* 30 (2018) 1703027.
- Y. Wang, C. Chen, H. Xie, T. Gao, Y. Yao, G. Pastel, X. Han, Y. Li, J. Zhao, K.K. Fu, L. Hu, *Adv. Funct. Mater.* 27 (2017) 1703140.
- M. Hilder, B. Winther-Jensen, N.B. Clark, *J. Power Sources* 194 (2009) 1135–1141.
- S.D. Lacey, D.J. Kirsch, Y. Li, J.T. Morgenstern, B.C. Zerket, Y. Yao, J. Dai, L.Q. Garcia, B. Liu, T. Gao, S. Xu, S.R. Raghavan, J.W. Connell, Y. Lin, L. Hu, *Adv. Mater.* 30 (2018) 1705651.
- K. Shen, H. Mei, B. Li, J. Ding, S. Yang, *Adv. Energy Mater.* 8 (2018) 1701527.
- X. Yang, H. Zhang, Y. Chen, Y. Yu, X. Li, H. Zhang, *Nano Energy* 39 (2017) 418–428.
- Y. Liu, G. Li, J. Fu, Z. Chen, X. Peng, *Angew. Chem. Int. Ed.* 56 (2017) 6176–6180.
- J. Song, M.L. Gordin, T. Xu, S. Chen, Z. Yu, H. Sohn, J. Lu, Y. Ren, Y. Duan, D. Wang, *Angew. Chem. Int. Ed.* 54 (2015) 4325–4329.
- Y. Ma, H. Zhang, B. Wu, M. Wang, X. Li, H. Zhang, *Sci. Rep.* 5 (2015) 14949.
- J.S. Kim, T.H. Hwang, B.G. Kim, J. Min, J.W. Choi, *Adv. Funct. Mater.* 24 (2014) 5359–5367.
- Y. Zhao, M. Li, Z. Yuan, X. Li, H. Zhang, I.F.J. Vankelecom, *Adv. Funct. Mater.* 26 (2016) 210–218.
- Y. Zhao, X. Yang, L.Y. Kuo, P. Kaghazchi, Q. Sun, J. Liang, B. Wang, A. Lushington, R. Li, H. Zhang, X. Sun, *Small* 14 (2018) 1703717.
- L. Wang, Y.-B. He, L. Shen, D. Lei, J. Ma, H. Ye, K. Shi, B. Li, F. Kang, *Nano Energy* 50 (2018) 367–375.
- Y.S. Su, A. Manthiram, *Nat. Commun.* 3 (2012) 1166.
- F.B. Holness, A.D. Price, *Smart Mater. Struct.* 27 (2018) 015006.
- N. Dagalakis, J. Flink, P. Stasikelis, J.F. Burke, I.V. Yannas, *J. Biomed. Mater. Res.* 14 (1980) 511–528.
- G. Ma, Z. Wen, Q. Wang, C. Shen, J. Jin, X. Wu, *J. Mater. Chem. A* 2 (2014) 19355–19359.
- R. Fang, S. Zhao, P. Hou, M. Cheng, S. Wang, H.M. Cheng, C. Liu, F. Li, *Adv. Mater.* 28 (2016) 3374–3382.
- M. Agrawal, S. Choudhury, K. Gruber, F. Simon, D. Fischer, V. Albrecht, M. Göbel, S. Koller, M. Stamm, L. Ionov, *J. Power Sources* 261 (2014) 363–370.
- X. Li, Q. Sun, J. Liu, B. Xiao, R. Li, X. Sun, *J. Power Sources* 302 (2016) 174–179.
- X. Yang, B. Dong, H. Zhang, R. Ge, Y. Gao, H. Zhang, *RSC Adv.* 5 (2015) 86137–86143.
- X. Yang, Y. Yu, N. Yan, H. Zhang, X. Li, H. Zhang, *J. Mater. Chem. A* 4 (2016) 5965–5972.
- G. Li, J. Sun, W. Hou, S. Jiang, Y. Huang, J. Geng, *Nat. Commun.* 7 (2016) 10601.
- Y. Cheng, K. Feng, W. Zhou, H. Zhang, X. Li, H. Zhang, *Dalton Trans.* 44 (2015) 17579–17586.
- Y. Yan, M. Shi, Y. Wei, C. Zhao, M. Carnie, R. Yang, Y. Xu, *J. Alloy. Compd.* 38 (2018) 16–24.
- D.R. Deng, T.H. An, Y.J. Li, Q.H. Wu, M.S. Zheng, Q.F. Dong, *J. Mater. Chem. A* 4 (2016) 16184–16190.
- K. Fu, Y. Wang, C. Yan, Y. Yao, Y. Chen, J. Dai, S. Lacey, Y. Wang, J. Wan, T. Li, Z. Wang, Y. Xu, L. Hu, *Adv. Mater.* 28 (2016) 2587–2594.
- R.R. Kohlmeier, A.J. Blake, J.O. Hardin, E.A. Carmona, J. Carpena-Núñez, B. Maruyama, J. Daniel Berrigan, H. Huang, M.F. Durstock, *J. Mater. Chem. A* 4 (2016) 16856–16864.
- J. Liu, B. Ludwig, Y. Liu, Z. Zheng, F. Wang, M. Tang, J. Wang, J. Wang, H. Pan, Y. Wang, *Adv. Mater. Technol.* 2 (2017) 1700106.



**Xuejie Gao** is currently a Ph.D. candidate in Prof. Xueliang (Andy) Sun's group at the University of Western Ontario, Canada. She received her B.S. degree in chemistry in 2014 from Ludong University and obtained her M.S. degree in Chemistry in 2017 from Soochow University. Currently, her research interests focus on the development of 3D printing applied for lithium batteries. She is also co-supervised by Prof. T. K. Sham from Chemistry Department in the University of Western Ontario. Part of her work is related to the study of energy materials via synchrotron radiation.



**Weihan Li** completed his doctorate in material sciences under the supervision of Prof. Yan Yu at the University of Science and Technology of China, Hefei in 2016. He is currently a postdoctoral fellow at Prof. Xueliang (Andy) Sun's Nanomaterials and Energy Group at the University of Western Ontario, Canada. His research interests mainly include synthesis and application of nanomaterials for lithium-ion battery and sodium-ion battery.



**Qian Sun** is a postdoctoral associate in Prof. Xueliang (Andy) Sun's Group at the University of Western Ontario (Western University), Canada. He received his B.S. degree in Chemistry in 2006, M.S. degree in Physical Chemistry in 2009, and Ph.D. degree in Applied Chemistry in 2013 under the supervision of Prof. Dr. Zheng-Wen Fu on the study of Li-/Na-ion batteries and Na-air batteries, all at Fudan University, China. He joined Prof. Sun's group in 2013 and his current research interests focus on Na-air, Na-ion, and room temperature Na-S batteries as well as solid-state Li/Na batteries.



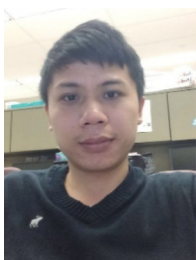
**Jianwen Liang** received his Ph.D. degree in inorganic chemistry from University of Science and Technology of China in 2015. He is currently a postdoctoral fellow in Prof. Xueliang (Andy) Sun's Nanomaterials and Energy Group at the University of Western Ontario, Canada. His research interests include sulfide-based solid-state electrolyte as well as all-solid-state Li/Li-ion batteries.



**Xiaofei Yang** is currently a postdoctoral associate in Prof. Xueliang (Andy) Sun's Nanomaterials and Energy Group. He received his B.E. degree in Chemical Engineering from Anhui University, China, in 2013 and Ph.D. degree in Dalian Institute of Chemical Physics, Chinese Academy of Sciences, China, in 2018 under the supervision of Prof. Huamin Zhang. His research interests focus on Li-S batteries, all-solid-state Li-S batteries and battery interface studies via synchrotron X-ray characterizations.



**Jiwei Wang** is currently a Ph.D. candidate in Prof. Xueliang (Andy) Sun's group at the University of Western Ontario, Canada. He is also co-supervised by Prof. T.K. Sham from Chemistry Department at the University of Western Ontario. He received his Bachelor degree in 2012 at the East China University of Science and Technology, and the Master degree in 2015 at Soochow University. His research interests focus on the three dimensional (3D) printing of high energy density lithium/sodium electrodes as well as all-printed solid-state batteries.



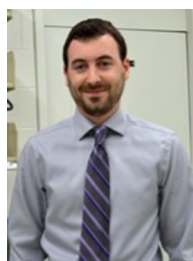
**Jianneng Liang** is currently a Ph.D. candidate in the department of Mechanical and Materials Engineering at the University of Western Ontario, Canada. He got his B.S. in metallurgical engineering in 2015 from Central South University, China. Currently, his research interests include solid-state polymer electrolytes, hybrid electrolyte, all-solid-state LIBs and Li-S batteries, and the interfacial study in all-solid-state batteries.



**Ruying Li** is a research engineer at Prof. Xueliang (Andy) Sun's Nanomaterial and Energy Group at the University of Western Ontario, Canada. She received her master in Material Chemistry under the direction of Prof. George Thompson in 1999 at University of Manchester, UK, followed by work as a research assistant under the direction of Prof. Keith Mitchell at the University of British Columbia and under the direction of Prof. Jean-Pol Dodelet at l'Institut national de la recherche Scientifique (INRS), Canada. Her current research interests are associated with synthesis and characterization of nanomaterials for electrochemical energy storage and conversion.



**Alicia Koo** received her B.Sc. in Chemistry at the University of British Columbia in 2016. Her research interests include energy conversion and storage materials for green energy applications. In addition, she is an avid science communicator and advocate for women in STEM.



**Frederick Benjamin Holness** is currently a Ph.D. student in Prof. Aaron Price's Organic Mechatronics and Smart Materials Laboratory at the University of Western Ontario, Canada. He received his B.Esc. degree in 2015 and M.Esc. degree in 2017 from the University of Western Ontario. Currently, his research interests focus on the development of additive manufacturing techniques for nanostructured conjugated polymer actuators and sensors.



**Aaron D. Price** is an Assistant Professor in the Department of Mechanical & Materials Engineering at Western University, where he leads the Organic Mechatronics and Smart Materials Laboratory. This NSERC-funded facility is equipped with a suite of additive manufacturing platforms and polymerization apparatus for the synthesis and fabrication of devices incorporating electrochemically active polymers. And his group developed new materials and advanced manufacturing technologies to achieve the first-ever 3D-printed polyaniline transducers realized through multi-material additive manufacturing and the first-ever micro-scale 3D polypyrrole transducers realized through digital light processing.



**T. K. Sham**, Fellow of the Royal Society of Canada and Officer of the Order of Canada, is a Distinguished University Professor and a Canada Research Chair at The University of Western Ontario. He obtained his Ph.D. with a B.Sc. from the Chinese University of Hong Kong. He was on the staff at Brookhaven National Laboratory for a decade before returning to Western in 1988. He was a founder of the Canadian Light Source and the Director of the Soochow-Western Centre for Synchrotron Radiation Research. Recent interests are in situ/in operando studies, nanomaterials, micro-beam X-ray analysis of cultural and heritage materials.



**Songlin Yang** is currently a Ph.D. candidate in the Chemical and Biochemical Engineering department at the University of Western Ontario, Canada. He received his B.E. degree of materials science and engineering in Tianjin University, China and MEng degree in University of Western Ontario, Canada. Currently, his research topic is the application of graphene nanocomposites and the fabrication of graphene biosensor.



**Xueliang (Andy) Sun** is a Canada Research Chair in Development of Nanomaterials for Clean Energy, Fellow of the Royal Society of Canada and Canadian Academy of Engineering and Full Professor at the University of Western Ontario, Canada. Dr. Sun received his Ph.D. in materials chemistry in 1999 from the University of Manchester, UK, which he followed up by working as a postdoctoral fellow at the University of British Columbia, Canada and as a Research Associate at L'Institut National de la Recherche Scientifique (INRS), Canada. His current research interests are focused on advanced materials for electrochemical energy storage and conversion.